0026-895X/04/6605-1169–1179$20.00
MOLECULAR PHARMACOLOGY
Copyright © 2004 The American Society for Pharmacology and Experimental Therapeutics
Mol Pharmacol 66:1169–1179, 2004

Vol. 66, No. 5
1420/1179635
Printed in U.S.A.

A Three-Dimensional Model for the Substrate Binding Domain of the Multidrug ATP Binding Cassette Transporter LmrA

Gerhard F. Ecker, Karin Pleban, Stephan Kopp, Edina Csaszar, Gerrit J. Poelarends,[1] Monique Putman, Dominik Kaiser, Wil N. Konings, and Peter Chiba

Institute of Medical Chemistry (S.K., P.C.), Medical University of Vienna, Department of Pharmaceutical Chemistry (G.F.E., K.P., D.K.), and the Mass Spectrometry Unit (E.C.), University of Vienna, Vienna, Austria; and Department of Microbiology, Groningen Biomolecular Sciences and Biotechnology Institute, University of Groningen, Groningen, the Netherlands (G.J.P., M.P., W.N.K.)

Received April 14, 2004; accepted August 5, 2004

ABSTRACT

Multidrug resistance presents a major obstacle to the treatment of infectious diseases and cancer. LmrA, a bacterial ATP-dependent multidrug transporter, mediates efflux of hydrophobic cationic substrates, including antibiotics. The substrate-binding domain of LmrA was identified by using photo-affinity ligands, proteolytic degradation of LmrA, and identification of ligand-modified peptide fragments with matrix-assisted laser desorption ionization/time of flight mass spectrometry. In the nonenergized state, labeling occurred in the α-helical transmembrane segments (TM) 3, 5 and 6 of the membrane-spanning domain. Upon nucleotide binding, the accessibility of TM5 for substrates increased, whereas that of TM6 decreased. Inverse changes were observed upon ATP-hydrolysis. An atomic-detail model of dimeric LmrA was generated based on the template structure of the homologous transporter MsbA from *Vibrio cholerae*, allowing a three-dimensional visualization of the substrate-binding domain. Labeling of TM3 of one monomer occurred in a predicted area of contact with TM5 or TM6 of the opposite monomer, indicating substrate-binding at the monomer/monomer interface. Inverse changes in the reactivity of TM segments 5 and 6 suggest that substrate binding and release involves a repositioning of these helices during the catalytic cycle.

Multidrug resistance in pro- and eukaryotic cells is often associated with enhanced expression of drug efflux proteins. LmrA, the first ATP-dependent multidrug efflux transporter identified in prokaryotes (van Veen et al., 1996), mediates resistance to a variety of lipophilic toxic compounds and antibiotics in *Lactococcus lactis*. LmrA is a structural and functional homolog of the human multidrug transporter P-glycoprotein (P-gp) (van Veen et al., 1998), which has been identified to play a major role for drug resistance in human tumors (Gottesman and Pastan, 1993) and of MsbA, a lipid transporter from *Escherichia coli* (Reuter et al., 2003). LmrA, P-gp, and MsbA have been demonstrated to have a similar substrate and modulator profile. Overexpression of LmrA resulted in increased resistance to 17 of 21 antibiotics, including broad-spectrum antibiotics belonging to the classes of aminoglycosides, lincosamides, macrolides, quinolones, streptogramins, and tetracyclines (Putman et al., 2000). Both LmrA and P-gp consist of two transmembrane domains, which are responsible for solute transport, and two ATP-hydrolyzing nucleotide-binding domains. In P-gp, all four domains are expressed as a single polypeptide chain, whereas in LmrA, monomers composed of a membrane domain fused to a nucleotide binding domain form a functional homodimer (van Veen et al., 2000). Electron cryomicroscopy studies indicated that, during the transport cycle, P-gp can adopt three different metastable conformations (Rosenberg et al., 2001). One of these conformations is observed in the

This work was supported by grant 17014 from the Austrian Science Fund (Fonds zur Förderung der Wissenschaftlichen Forschung) and grant 10654 from the Austrian National Bank.
W. N. K and P. C. contributed equally to this work.
The coordinates of the LmrA model are available from the authors upon request.
[1] Current address: Division of Medicinal Chemistry, College of Pharmacy, University of Texas, Austin, Texas
Article, publication date, and citation information can be found at http://molpharm.aspetjournals.org.
doi:10.1124/mol.104.001420.

ABBREVIATIONS: P-gp, P-glycoprotein; AMP-PNP, adenyl-5′-yl imidodiphosphate; ATR-FTIR, attenuated total reflection Fourier transform infrared spectroscopy; MALDI-TOF, matrix-assisted laser desorption ionization/time-of-flight; ABC, ATP binding cassette; TM, transmembrane segment; TFA, trifluoroacetic acid; CHCA, α-cyano-4-hydroxycinnamic acid; Vc-MsbA, bacterial lipid transporter MsbA from *V. cholerae*; Eco-MsbA, bacterial lipid transporter MsbA from *E. coli*; AA, amino acids; TMD, transmembrane domain; NBD, nucleotide-binding domain; ICD, intracellular domain; PAGE, polyacrylamide gel electrophoresis.

nonenergized state, a second upon ATP-binding. Hydrolysis does not seem to be required, because a nonhydrolysable analog of ATP, AMP-PNP, can substitute for ATP in eliciting this conformational change. If this conformational change affords substrate affinity has been disputed (Martin et al., 2001; Sauna and Ambudkar, 2001; Loo and Clarke, 2002; Al-Shawi et al., 2003).

A third conformation is observed in the ADP/vanadate blocked posthydrolytic state. Similar structural changes, reflected by changes in the protein secondary structure, have been demonstrated for P-gp by site-directed mutagenesis and subsequent cross-linking studies of P-gp (Loo and Clarke, 2001; Loo et al., 2003) and for LmrA by attenuated total reflection Fourier transform infrared spectroscopy (ATR-FTIR) (Grimard et al., 2001). Furthermore, binding and heterologous displacement studies revealed the presence of two allosterically interacting substrate binding sites in dimeric LmrA. Only one of these sites is accessible in the ADP/vanadate-blocked state (van Veen et al., 2000). These studies have led to the postulation of an alternating two-site transport model for LmrA (van Veen et al., 2000).

However, the molecular basis for drug recognition and the three dimensional structure of the drug binding sites remain elusive. In the present study, a set of substrate photoaffinity ligands related to the lead compound propafenone have been used to label LmrA at different steps of the transport cycle. Ligand-labeled peptide fragments were identified by MALDI-TOF-mass spectrometry. Lack of atomic resolution data for LmrA precluded relating this information to the 3D structure of the protein. However, structures of full-length ABC transporters have become available recently. These are BtuCD, the vitamine B12 transporter from *E. coli* (Locher et al., 2002) and the essential bacterial lipid transporter MsbA (Chang and Roth, 2001). Because the number of membrane-spanning helices in BtuCD does not correspond with the predicted six TM helices in LmrA, this structure does not provide a useful template for homology modeling. In contrast, MsbA has a strong sequence homology (48% amino acid residues with strong similarity, 30% identity) with LmrA and the number of TM helices agrees with that predicted for LmrA. The first MsbA structure to become available was that from *E. coli* (Eco-MsbA). However, the comparatively low resolution (4.5 Å, Cα-trace only), the high number of missing residues (a total of 23% of its AA residues are missing), and a dimer interface that probably represents a consequence of crystal packing precluded the use of this structure as a template for direct homology modeling. Molecular dynamics simulation studies subsequently led to an improved Eco-MsbA template (Campbell et al., 2003). A high-resolution crystallographic structure of *Vibrio cholerae* MsbA (Vc-MsbA) has recently become available (Chang, 2003). This structure has a 3.8-Å resolution and a low number of missing residues. The structure contains nearly all side chains, and the monomer/monomer interface probably represents a physiologically relevant conformation. Access to this high-resolution protein structure allowed generation of a homology model for LmrA. The information obtained by photoaffinity labeling studies was projected onto this model, suggesting two rotationally symmetric substrate binding domains per LmrA dimer. The substrates are bound at the monomer/monomer interface and involve TM3 of one monomer and TM5 and -6 of the other monomer. Changes in the labeling pattern during the catalytic cycle indicate a repositioning of helices 5 and 6.

Materials and Methods

Design and Synthesis of Compounds. The design and synthesis of propafenone-type compounds including the photo-affinity ligands has been described previously (Chiba et al., 1995, 1996; Ecker et al., 2002). Structures were confirmed by IR, mass spectroscopy, NMR spectroscopy, and elemental analysis. Structures of the photoaffinity ligands are presented in Table 2. [^{3}H]GPV51 (110 mCi/ml, 5.5 mM) was obtained by tritium gas exchange (PerkinElmer Life and Analytical Sciences, Boston, MA).

Bacterial Strains and Expression Vector. *Lactococcus lactis* NZ9000 (lmrA$^-$), which lacks the gene encoding the multidrug transporter LmrA (obtained from J. Kok, Department of Genetics, University of Groningen), was used in combination with the nisin-controlled expression (NICE) system (de Ruyter et al., 1996) for overexpression of LmrA. *L. lactis* NZ9700 was used as a nisin-producing strain. The cells were grown at 30°C in M17 medium (Difco, Detroit, MI) supplemented with 0.5% glucose and 5 μg/ml chloramphenicol when appropriate. Expression of LmrA mutants from pNZ8048-derived plasmids (obtained from Dr. O. Kuipers, NIZO, Ede, The Netherlands) was induced by adding 40 ng/ml nisin at an OD_{660} of about 0.8, and cells were harvested 1.5 h after induction.

Cytotoxicity Assays. Propafenone analogs were studied for its substrate properties toward LmrA in cytotoxicity assays. Toxicity in *E. coli* CS1562 cells overexpressing the transporter was compared with that in control CS1562 cells not expressing LmrA. Strain CS1562 (*tolC6*::*Tn10*) was used in these assays because it is hypersensitive to drugs owing to a deficiency in the TolC protein, resulting in an impaired barrier function of the outer membrane (Austin et al., 1990).

Preparation of Membrane Vesicles. Inside-out membrane vesicles were prepared by passage through a French pressure cell as described previously (Margolles et al., 1999; Poelarends et al., 2000). The vesicles were frozen in liquid nitrogen and stored at −80°C at a protein concentration of 20 mg/ml in 50 mM Tris-HCl and 1 mM EDTA, pH 7.4, containing 10% glycerol. The protein concentration was determined with a detergent-compatible protein assay (Bio-Rad, Vienna, Austria).

Photolabeling of LmrA and Gel Electrophoretic Separation Conditions. Inside-out membrane-vesicles were taken up in 50 mM Tris-HCl, pH 7.4, and preincubated with ligand at a concentration of 10 nM unless indicated otherwise. [^{3}H]GPV51 (5 μCi) was added to give a final concentration of 2.75 μM. Samples were preincubated at room temperature for 15 min. Mg-AMP-PNP was added at a concentration of 2 mM. The posthydrolytic transition state was trapped by addition of 2 mM Mg-ATP and 2 mM orthovanadate as described previously (van Veen et al., 2000). Preincubation conditions were identical to those described in (van Veen et al., 2000). Samples were placed on ice and irradiated with a 500-W mercury lamp (Lot-Oriel, Darmstadt, Germany) 6 times for 30 s, with 30-s pauses between the irradiation cycles, in the presence and absence of the photoactivatable propafenones. A 1-mm glass plate was placed in the light path to filter most of the UV light with wavelengths below 300 nm. For competition experiments with radio-labeled GPV51, unlabeled GPV51 was added at the concentrations indicated in Fig. 1. After irradiation, samples were centrifuged at 50,000*g* for 30 min at 4°C. Protein pellets (30 μg of total plasma protein per lane) were taken up in 1× SDS/sample buffer, loaded on a 10% polyacrylamide gel, and run at 35 mA for 60 min using a Hoefer Mighty Small II SE250 unit (Amersham Biosciences, Vienna, Austria). Gels were fixed in methanol/glacial acetic acid/water (50:10:40) for 30 min, washed overnight in double-distilled water, and soaked in Amplify (Amersham Biosciences) for 30 min. Gels were dried for 2 h in a vacuum gel dryer

(Bio-Rad) at 80°C and subjected to fluorography using an Amersham ECL Hyperfilm.

Chemicals for in-Gel Digestion and Mass Spectrometry. High-quality water for the in-gel digestion and the mass spectrometric experiments was prepared using a Milli-Q water purification system (Millipore, Bedford, MA). Ammonium hydrogen carbonate was obtained from FLUKA (Sigma-Aldrich, Vienna, Austria), dithiothreitol for the reduction of proteins before in-gel digestion was purchased from Novex (San Diego, CA), iodoacetamide was supplied by Sigma (Vienna, Austria), trypsin and chymotrypsin were obtained from Roche (sequencing grade; Roche Diagnostics GmbH, Mannheim, Germany). Acetone was from AppliChem (Darmstadt, Germany), acetonitrile, methanol, and isopropanol (high-performance liquid chromatography grade) were purchased from Sigma, trifluoroacetic acid (TFA) was obtained from Pierce (Rockford, IL), and formic acid was supplied by VWR (VWR Intl, Darmstadt, Germany). The α-cyano-4-hydroxycinnamic acid (CHCA) matrix for the MALDI-TOF measurements was purchased from Bruker (Bruker Daltonik GmbH, Bremen, Germany) and used without further purification. Nitrocellulose was purchased from Bio-Rad. Protein and peptide standards used to calibrate the MALDI mass spectrometer were obtained from Bruker.

Silver Staining and in-Gel Digestion. Proteins were visualized by silver-staining according to the method of Shevchenko et al. (1996), and the in-gel digestion was performed without destaining of the gel as described in Durauer et al. (2000).

MALDI-TOF Mass Spectrometry. A Bruker REFLEX III MALDI-TOF instrument, equipped with a standard nitrogen laser (337 nm) was used for mass spectrometry. The spectra were recorded in reflectron mode, positive ionization, and with an acceleration voltage of 25 kV. The laser power was varied on a relative scale of 0 to 100 and was kept at the threshold value to obtain appropriate signal intensity. The calibration of the instrument was done externally. Samples were prepared with a 75:25 (v/v) mixture of CHCA matrix (saturated solution in acetone) and nitrocellulose [10 mg/ml solution in acetone/isopropanol 50:50 (v/v)]. A 1-μl aliquot of the mixture was placed onto the sample slide and allowed to dry at room temperature. In-gel–digested LmrA (0.5 μl) was mixed with 0.5 μl of 0.1% TFA on this thin layer of matrix crystals and vacuum-dried.

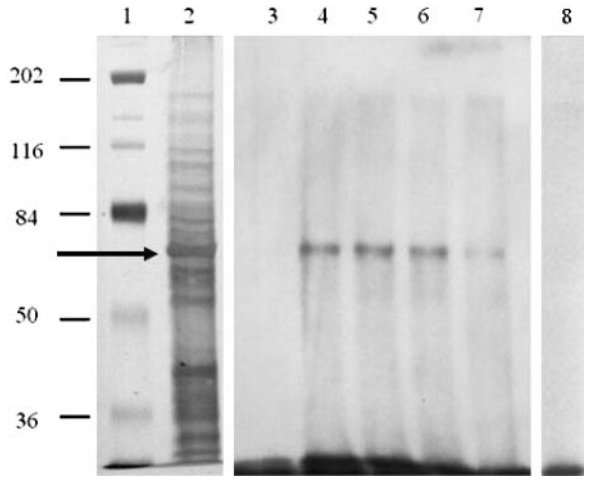

Fig. 1. Photolabeling of LmrA with the radioligand [^{3}H]GPV51. Inside-out membrane vesicles of LmrA overexpressing *L. lactis* NZ9000 were irradiated at a photoligand concentration of 2.75 μM. Membrane proteins were separated on a 10% SDS-polyacrylamide gel. Lane 1, molecular mass marker; lane 2, silver stain of total membrane protein (the LmrA band is indicated by an arrow); lanes 3 to 7, fluorography; lane 3, unirradiated control; lane 4, sample irradiated in the presence of 2.75 μM [^{3}H]GPV51; lanes 5 to 7, same as 4, but irradiated in the presence of 2.75 μM radioactive GPV51 plus unlabeled GPV51 at a concentration of 50 μM (lane 5), 150 μM (lane 6), and 500 μM (lane 7); lane 8, empty vector transfected *L. lactis* irradiated in the presence of radioligand.

Samples were washed with ice-cold 0.1% TFA. Hydrophobic peptides were purified and concentrated on Poros 20 R1 material (Applied Biosystems, Foster City, CA) loaded into GeLoader tips (Eppendorf-Netheler-Hinz-GmbH, Hamburg, Germany). The chromatography material was conditioned with 0.1% TFA and the peptides were eluted with CHCA matrix [saturated solution in 0.1% TFA/acetonitrile 50:50 (v/v)] directly onto the sample slide. Each spectrum was produced by accumulating data from 90 to 120 consecutive laser shots. Spectra were interpreted with the aid of the Mascot (Matrix Science Ltd, London, UK) or MS-Fit (Clauser et al., 1999) software using the NR database (NCBI Resources, National Institutes of Health, Bethesda, MD). Ligand modified masses were matched to peptide masses generated by *in silico* digests of the protein with the aid of a custom program developed in our laboratory.

Data Analysis. Statistical analysis was perfomed using the unpaired Student's *t* test with a 95% confidence interval for the sample mean. There were six independent observations.

Modeling of LmrA Using Vc-MsbA as Template. The crystal structure of Vc-MsbA has recently been determined at a resolution of 3.8 Å (Chang, 2003). Crystals were obtained in the absence of nucleotide. Unlike in the crystal structure of MsbA from *E. coli* (Chang and Roth, 2001), which represents only a Cα trace, most of the side-chain positions of Vc-MsbA have been determined. The nucleotide binding domain was resolved with the exception of AAs 565–582. The observed dimer position was different from the previously published Eco-MsbA and in agreement with the low resolution electron microscopy data of the homologous human multidrug transporter P-glycoprotein (Rosenberg et al., 2001, 2003). The TMD is completely resolved except for the first 14 N-terminal amino acid residues and amino acids 203 to 237. The latter are located in the loop connecting TM helices 4 and 5.

The sequence of LmrA was aligned with Vc-MsbA using the Align123 module of the software package InsightII. As a matrix, we chose the Blosum62 matrix with a gap penalty of 11, a gap extension penalty of 1, and the "remove gaps" option. The alignment was carefully checked to avoid deletions or insertions in conserved regions and in transmembrane segments. In addition, the alignments of P and G residues were checked to get the best possible fit. Because of a deletion in ECL1 (connecting TM helices 1 and 2), a new loop was generated that adopts a conformation different from the ECL1 in Vc-MsbA. Because the N-terminal 14 amino acid residues and the region referred to as the intracellular loop 2 (ICL2, AA positions 203–237) have not been resolved in Vc-MsbA, corresponding amino acids in the LmrA sequence (Met1–Ser20 and Phe210–Leu244)) were removed. The LmrA sequence was subsequently divided into two fragments (Ile21-Nle209 and Tyr245-Glu570) that were assigned to the respective coordinates of Vc-MsbA separately, so as not to yield a virtual bond between Nle209 and Tyr245). Both LmrA fragments were energy-minimized at splice points with a cycle of 500 steps Steepest Descent Algorithm minimization (derivative 1 Å). To yield a complete LmrA monomer, the two fragments were merged. In addition, some residues of Vc-MsbA have been determined without side chain positions. These side chains were predicted in the Biopolymer mode of InsightII before minimization. The structural quality of the model was assessed by a structure check using ProStat. For the final dimer assembly, two LmrA monomers were fitted onto the Vc-MsbA dimer by least square superposition, yielding an LmrA model in a closed conformation.

Results

Propafenones Are Transported Substrates (Allocrites) of LmrA. The aim of this study was to obtain information about the substrate binding domain of LmrA, the ABC multidrug transporter of *Lactococcus lactis,* by studying the interaction of LmrA with propafenone-type photoaffinity ligands. To investigate whether the lead compound

propafenone and its analogs are substrates for LmrA, their toxicities were studied in LmrA overexpressing *E. coli* CS1562 cells and compared with those obtained in parental *E.coli* CS1562 cells as described previously (Putman et al., 2000). Table 1 gives IC_{50} values of propafenone analogs obtained in empty vector-transfected cells and in cells transfected with the LmrA containing plasmid pGKLmrA. Overexpression of LmrA resulted in resistance toward the *R*- and *S*-enantiomers of the parental compound propafenone and its analogs, including the benzophenone-type photoligand GP317 (Table 1). These data indicate that propafenones are substrates for LmrA. This conclusion was further confirmed by the dose-dependent inhibition by propafenones of transport of Hoechst 33342, a well established substrate of LmrA, in inside-out membrane vesicles of LmrA overexpressing *L. lactis* NZ9000 (data not shown).

Propafenones Bind to LmrA. The interaction of LmrA with propafenone-type photoaffinity ligands was studied by using compound GPV51 (Table 2), radio-labeled by tritium gas exchange. Inside-out membrane vesicles of *L. lactis,* overexpressing LmrA, were irradiated in the presence of [^{3}H]GPV51, and membrane proteins were separated by SDS-PAGE. Fluorographs revealed a single photolabeled band (Fig. 1, lane 4) at approximately 64 kDa, which was confirmed to represent LmrA by Western blotting. This band was absent in parental cells irradiated in the presence of [^{3}H]GPV51 (Fig. 1, lane 8). Other proteins were not labeled to any significant extent. The LmrA band was absent in nonirradiated samples (Fig. 1, lane 3). The simultaneous presence of nonradioactive GPV51 decreased radiolabeling in a dose-dependent manner (Fig. 1, lanes 5–7) indicating specificity of the photolabeling reaction. Similarly, the known LmrA substrates ethidium bromide and Hoechst 33342 competed with binding of [^{3}H]GPV51 in a dose-dependent manner, suggesting a common binding site or region of binding of these compounds (S. Kopp, G. F. Ecker and P. Chiba, unpublished observations).

Identification of Substrate-Binding Regions of LmrA. Inside-out membrane vesicles of LmrA-overexpressing *L. lactis* were photo-labeled with propafenone-type ligands. Structures of the photoligands are given in Table 2. Membrane proteins were separated by SDS-PAGE and the bands visualized by silver staining. The 64-kDa band corresponding to LmrA was excised and proteolytically degraded by chymotrypsin. Ligand labeled peptide fragments were identified by high resolution MALDI-TOF mass spectrometry. Because the efficiency of the photochemical reaction is low, the majority of mass peaks corresponded to unmodified peptide fragments. These covered the LmrA sequence along the full length of the protein. An assignment of mass peaks to LmrA was accomplished by comparison with a list of theoretical peptide masses obtained by *in silico* proteolytic degradation of the protein with chymotrypsin. For the identification of ligand-modified peptide, theoretical masses were increased by the ligand mass and then compared with yet unassigned masses. For ligand GPV51, these masses of ligand-modified peptide fragments are listed in Table 3. The ligand concentration in these experiments was 10 pM. Experimentally determined (submitted) masses (the sum of the peptide fragment mass and the ligand mass), predicted peptide fragment masses, mass accuracy in ppm, and start and end amino acids of the fragment, assignment, and sequence are given. A total of 16 ligand-modified peptide fragments (fragments 1–16) were identified to be located within the TMD. These were assigned to putative TM segments 3 (peptides 1–3), 5 (peptides 4–10, of which peptide 4 extends into the intracytoplasmic loop 2), and 6 (peptides 11–16). In addition, two peptides were assigned to the NBD (fragments 17 and 18). Of these, one fragment (Asp461-Phe468) was in the α-helical domain (also designated signaling domain) and one fragment contained the Walker B sequence (Arg503-Leu517). Overlap of some fragments was caused by incomplete cleavage at protease recognition sites. Partial modifications (partial oxidation of methionine residues and partial dehydration of the tertiary alcohol adduct of the photoreaction) were present in some fragments. Simultaneous detection of these partially oxidized and dehydrated peptide fragments (which are not listed in Table 3) indicated correct mass peak assignment. Additional reliability was introduced by repeating these experiments with five other photoligands of different masses. The rationale of these experiments was that peptide fragments, which are covalently modified by the photoligand, shift from their original position in the mass spectrum to an *m/z*, which is increased by the ligand mass. Because only a small fraction of the peptides is modified, two peaks are then detected, one at an *m/z* corresponding to the unmodified peptide and the other at an *m/z* corresponding to the sum of the masses of the peptide fragment and the ligand. With a certain probability, which is different from zero, a spurious peak might be present at this position in the mass spectrum, which might subsequently be identified as a ligand modified peptide. This probability, however, is indistinguishable from zero, when ligands of different masses are used and consensus binding regions are determined.

A tabular representation of data for the complete set of six photoligands (including fragments containing partially oxidized methionines and fragments in which the photolabeling adduct was dehydrated) would be complex to view. Therefore data are shown in an easily comprehensible graphical representation. The number of fragments containing a particular

TABLE 1
Propafenone analogs

Substance	IC_{50}		Fold Resistance	Reference (Substance Code)
	CS1562/pGK13	CS1562/pGKLmrA		
	μM			
(*R*)-Propafenone	51	443	8.7	Chiba et al., 1995 (1a)
(*S*)-Propafenone	52	430	8.3	Chiba et al., 1995 (1a)
GPV02	96	1266	13.2	Chiba et al., 1995 (1d)
GPV03	93	1181	12.7	Chiba et al., 1996 (03)
GPV09	137	1772	12.9	Chiba et al., 1995 (1e)
GPV317	43	732	17.0	Ecker et al., 2002 (GP317)

TABLE 2
Chemical structure of benzophenone-type photoligands

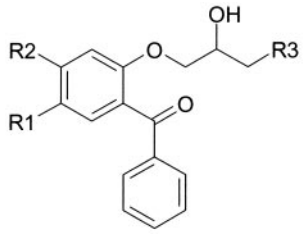

Compound	R1	R2	R3	Exact Mass
GPV 51	H	H	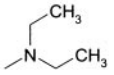	327.183
GPV 317	H	H	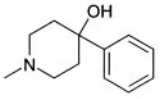	431.210
GPV 319	H	H	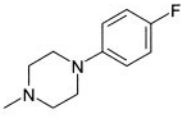	434.200
GPV 442	-CH_3	H	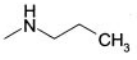	327.183
GPV 708	H	H	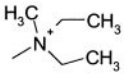	342.210
BP 11	H	-OCH_3		369.194

amino acid was counted and plotted as a function of the amino acid position. The frequency distribution of photolabeled fragments obtained for nonenergized LmrA is shown in Fig. 2A. The data presentation is exemplified for tyrosine residue 297: Table 3 shows Y297 in TM6 to be contained in six fragments modified by ligand GPV51. When repeating this experiment with five additional photoligands, the number of modified peptide fragments can be expected to be 6-fold higher. As seen in Fig. 2A, additional consideration of partial modifications (methionine oxidations and dehydration of the postlabeling adduct) brings this number to 75 modified peptide fragments in which Y297 is contained.

Figure 2A shows that within the TMD, helices 3, 5, and 6 were preferentially labeled. TM segments 1, 2 and 4 were not modified to any significant extent, although peptide fragments from these TM segments were found in unmodified form. A bias for recovery of peptide fragments from these TM segments was not observed for unmodified peptide fragments. The propensity of benzophenone-type photoligands to react with methionine residues (Rihakova et al., 2002) is reflected by the fact that highest labeling is observed in methionine-containing sequences Gln169-Met170 in TM3, Leu268-Met269-Ile270 in TM5, and Met295-Met296-Tyr297 in TM6.

Photoaffinity labeling was also observed in the NBD. Highest labeling occurred in the α-helical domain (Schmitt and Tampe, 2002) between residues Tyr445 and Val469, a sequence stretch that does not contain methionine residues and, to a lesser extent, near Walker B, with Met509 as the peak-scoring amino acid. These data show that although methionine residues represent preferred reaction partners of benzophenone-type photoligands, they are not an absolute requirement for labeling. Furthermore, accessibility of methionine residues is a prerequisite for labeling. A number of methionine residues, such as those in TM4, are not labeled by the ligands, thus demonstrating that this helix is inaccessible to the ligands. Benzophenone itself did not label LmrA, indicating that the benzophenone moiety of the ligands alone

TABLE 3
Peptide fragments photolabeled by GPV51 as identified by MALDI-TOF mass spectrometry
Photolabeling, proteolysis with chymotrypsin and mass spectrometry was performed as described under *Materials and Methods*. GPV51 was used at a concentration of 10 pM. The experimentally determined (submitted) and predicted (matched) exact masses, mass accuracy, start and end amino acid (AA), localization, and sequence in one letter code are shown.

Fragment No.	[M + H$^+$]		Mass Accuracy	Start AA	End AA		Peptide Fragment
	Submitted	Matched					
	Da		*ppm*				
1	1993.028	1993.101	−37	146	158	TM3	IANSIPQAFTSIL
2	1289.687	1289.737	−39	161	166	TM3	VGSIIF
3	1937.948	1938.035	−45	167	176	TM3	MLQMQWRLTL
4	2374.206	2374.259	−22	246	264	ICL2/TM5	KIGVKEAVFDGLMSPVMML
5	1864.777	1864.876	−53	255	268	TM5	DGLMSPVMMLSMML
6	1597.706	1597.744	−24	258	268	TM5	MSPVMMLSMML
7	2159.130	2159.043	40	258	273	TM5	MSPVMMLSMMLMIFGL
8	1505.773	1505.826	−35	272	279	TM5	GLLAYGIY
9	2660.367	2660.463	−36	272	291	TM5	GLLAYGIYLISTGVMSLGTL
10	1927.944	1928.041	−51	274	288	TM5	LAYGIYLISTGVMSL
11	1456.819	1456.711	74	289	298	TM6	GTLLGMMMYL
12	1814.840	1814.878	−21	289	301	TM6	GTLLGMMMYLMNL
13	1072.497	1072.484	12	292	297	TM6	LGMMMY
14	1834.859	1834.898	−21	292	301	TM6	LGMMMYLMNL
15	959.476	959.405	74	293	297	TM6	GMMMY
16	2562.260	2562.279	−8	293	312	TM6	GMMMYLMNLIGVVPTVATFF
17	1253.642	1253.654	−9	461	468	NBD	DLAFARSF
18	2015.009	2015.085	−38	503	517	NBD	RNPKILMLDEATASL

is insufficient to mediate binding to the transporter (data not shown).

Photoaffinity Labeling of LmrA at Different Stages of the Transport Cycle. During allocrite transport, the TMDs are thought to undergo a sequence of conformational changes, during which their drug binding sites face alternately the intracellular side (or membrane environment) and the extracellular side of the membrane (or water filled cavity, which connects to the extracellular environment). Excretion of the cytotoxic substrates involves binding at a high affinity binding site(s), translocation and substrate release based on an affinity-decrease at the off-site(s).

To obtain information about the changes in substrate binding by LmrA, we labeled the protein with [^{3}H]GPV51 at different steps of the transport cycle (Fig. 3). The labeling intensity of the LmrA band was similar for samples prepared in the absence of nucleotide or in the presence of the nonhydrolyzable ATP-analog AMP-PNP (mimicking the ATP-bound state), but was approximately 70% reduced in the posthydrolytic ADP/vanadate-blocked transition state. Similar results were obtained in homologous displacement studies using [^{3}H]GPV51 and nonradioactive GPV51 (data not shown). Analogous observations were also made for the binding of the substrate vinblastine in the ADP/vanadate blocked transition state (van Veen et al., 2000) and for iodoarylazidoprazosine-labeled P-gp (Ramachandra et al., 1998).

In subsequent experiments, the labeling pattern with nonradioactive photo-ligands was determined in the absence or presence of AMP-PNP and in the posthydrolytic transition state. A pair-wise comparison of labeling patterns obtained at different steps of the transport cycle was performed. The principle of this comparison is illustrated in Fig. 2. Composite data for six ligands are shown. Predicted TM segments are indicated by numbers and shown as gray traces. As discussed before, the labeling pattern for the nonenergized state is represented in Fig. 2A, and the labeling pattern for the AMP-PNP-bound state is shown in Fig. 2B. For each amino acid position, the number of fragments obtained in the nonenergized state was subtracted from that in the AMP-PNP bound state. Hence, labeling increases result in positive peaks, whereas decreased labeling gives a negative peak (Fig. 2C). The area of the peak is a measure of changes in labeling intensity and reflects changes in the ligand accessibility of protein regions at different steps of the transport cycle. In this case, labeling of TM5 increased and that of TM6 decreased when proceeding from state A to state B. It is important to note that mathematical differences reflect changes in the ligand-accessibility of certain protein regions independent of other factors, such as photochemistry, cleavage site distribution, and potential variation in coverage of the protein across its length.

According to the above procedure, the pairwise comparison of labeling patterns at different steps of the transport cycle was performed. Results are shown in Fig. 4. Upon addition of AMP-PNP (Fig. 4A), the number of photo-labeled fragments

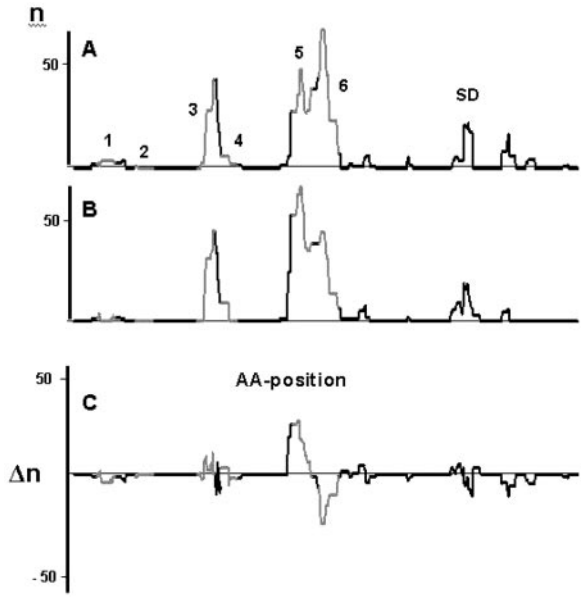

Fig. 2. A, frequency distribution analysis of photolabeling. Pooled data for six affinity ligands are shown. The number of labeled peptide fragments (n) containing a particular amino acid were counted and plotted as a function of this amino acid position. LmrA containing inside-out membrane vesicles were irradiated in the presence of six different photoligands. After SDS-PAGE, LmrA was localized by silver staining, the band was excised, and LmrA was proteolytically degraded with chymotrypsin. The masses of the resulting peptide fragments were determined by MALDI-TOF mass spectrometry as described under *Materials and Methods*. The TM segments are indicated by numbers and are shown in gray. SD denotes the position of the signaling domain (α-helical domain). B and C, exemplary illustration of the method of pair-wise comparison of the number of peptide fragments (n) obtained at different stages of the transport cycle. The labeling pattern in the nonenergized state (A) was compared with the labeling pattern in the AMP-PNP–bound state (B). The curve shown in C was obtained by calculating the mathematical differences (Δn) between state B and state A for each individual amino acid position. Pooled data for six ligands are shown. Positive peaks indicate increases in the number of fragments; negative peaks indicate decreases.

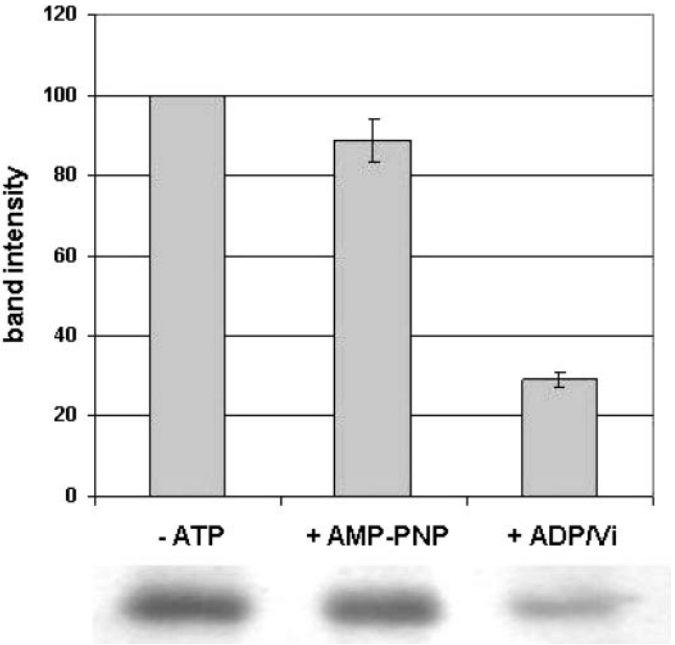

Fig. 3. Photolabeling of LmrA at different stages of the catalytic cycle. Inside-out membrane vesicles from LmrA overexpressing *L. lactis* NZ9000 were irradiated in the presence of the radioligand [^{3}H]GPV51 in the absence of ATP (nonenergized condition) or in the presence of 2 mM AMP-PNP or 2 mM ADP and 2 mM vanadate. Membrane proteins were separated on a 10% SDS-polyacrylamide gel and subjected to fluorography. The graph shows band intensities relative to the band obtained in the nonenergized state. Error bars indicate the standard deviation of three experiments. Intensity of the bands in fluorographs is shown below the bar graph.

assigned to TM5 increased, whereas that for TM6 decreased compared with labeling in the absence of nucleotide. The number of fragments assigned to TM3 remained essentially unaltered. Upon hydrolysis of ATP, a posthydrolytic transition state is reached that can be mimicked by ADP/vanadate trapping (van Veen et al., 2000). A comparison of the AMP-PNP-bound state with this posthydrolytic state revealed a decreased labeling of TM5 but an increased number of fragments assigned to TM6 (Fig. 4B). A comparison of the nonenergized state with the posthydrolytic state showed that these two states represent different conformations, because the number of peptide fragments for TM5 was lower and that

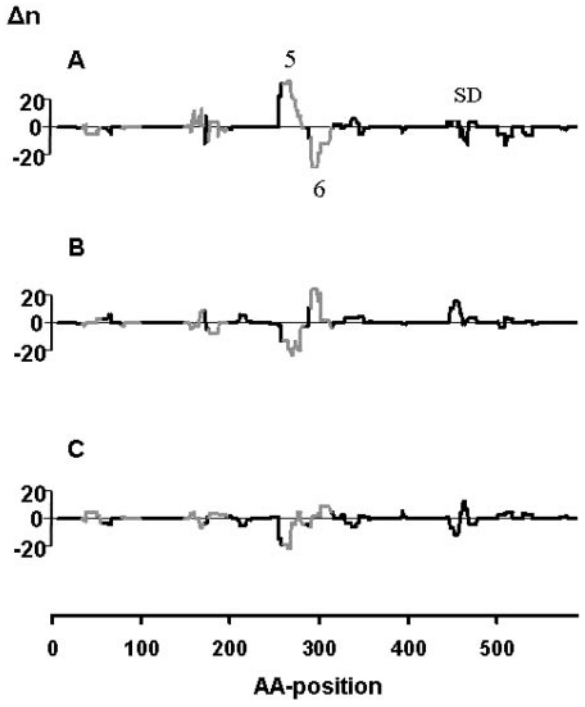

Fig. 4. Changes in the labeling pattern of LmrA after nucleotide binding and hydrolysis. Traces were obtained as described in Fig. 2. The amino acid position is given on the abscissa, and the change in the number of labeled peptide fragments (Δn) is on the ordinate. The following states were compared: A, AMP-PNP–bound versus nonenergized state; B, AMP-PNP–bound versus ADP/Vi blocked state; C, ADP/Vi-blocked versus nonenergized state. Positions of TM5 and -6 (TM segments shown as gray traces) and of the α-helical domain (SD, signaling domain) are indicated.

for TM6 was higher in the posthydrolytic transition state (Fig. 4C). For all labeling traces, the loop region between TMs 5 and 6 (shown in black) intersects with or is located near the abscissa, indicating that it does not change affinity toward the ligands during catalysis. Inspection of the NBD also shows labeling differences, which are less pronounced than those of the TMD. A signal is visible in the traces of Fig. 4, which is located between amino acid positions 445 and 469, indicating that this region undergoes conformational changes during the catalytic cycle, leading to differing ligand accessibility. This region corresponds to the α-helical domain (signaling domain SD), which has been proposed to represent the interface region between NBD and TMD (Schmitt and Tampe, 2002).

The statistical significance of the results presented in Fig. 4 was evaluated for the TMD by an unpaired Student's *t* test with a 95% confidence interval for the sample mean. Changes expressed as peak areas were evaluated for each ligand individually at each step of the transport cycle. The labeling-changes of TMs 5 (black columns) and 6 (gray columns) were found to be statistically significant when proceeding either from the nonenergized to the AMP-PNP–bound state (Fig. 5A, significant changes indicated by asterisk) and from the AMP-PNP–bound to the posthydrolytic transition state (Fig. 5B). Likewise, changes in labeling of TM5 and TM6 were statistically significant in a comparison of the nonenergized and posthydrolytic transition states (Fig. 5C). Changes in labeling of TM3 (open columns) were not statistically significant.

Generation of a Three-Dimensional Atomic Detail Model of LmrA. A protein homology model of LmrA was generated based on the template structure of dimeric *V. cholerae* MsbA as described under *Materials and Methods*. A detailed description of protein homology modeling will be published separately (Pleban et al., 2004). The quality of a homology model strongly depends on correct sequence alignment (Campbell et al., 2003). Therefore, alignments obtained by the "Align123" module of InsightII were carefully checked for deletions and insertions in structurally conserved regions and, if necessary, corrected manually. The resulting LmrA model correctly predicted that polar amino acid residues in TM segments were oriented toward the central pore whereas apolar residues were oriented toward the lipid bilayer, supporting a valid sequence alignment. In addition, the orienta-

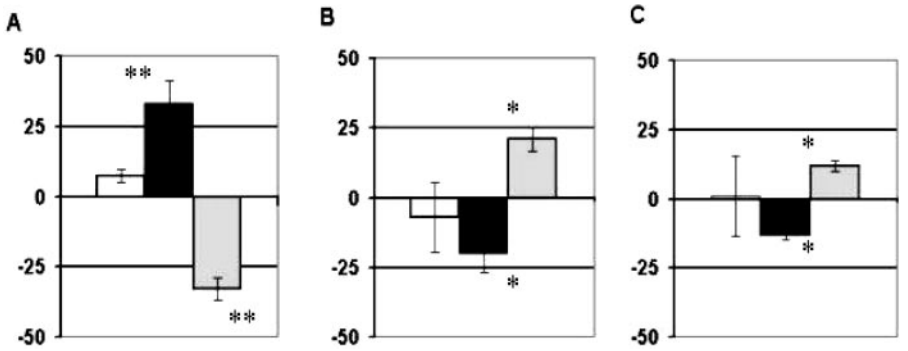

Fig. 5. For each of the six photoligands, traces such as those shown in Fig. 4 were obtained, and the peak area was determined as a measure of the change in labeling. The average peak areas are given. Error bars indicate the standard deviation. A–C, pair-wise comparison of states as shown in Fig. 5. The following changes were statistically significant (p values <0.05, Student's t test): changes in labeling of TM5 (open bars) and TM6 (black bars) between nonenergized and AMP-PNP–bound state (A); increased labeling of TM6 and decreased labeling of TM5 in the posthydrolytic state compared with the AMP-PNP–bound state (B); and posthydrolytic transition state compared with the nonenergized state (C). These changes are denoted by an asterisk. No statistically significant difference in the labeling of TM3 (gray bars) was found in either comparison of states.

tion of TM6 is compatible with previous cysteine scanning mutagenesis data, indicating that one side of TM6 is water accessible (Poelarends and Konings, 2002). Structural validation indicated that 99.3% of the residues (567 of 571 amino acids, the 15 N-terminal AA residues are not included in the model) had backbone torsion angles in the favored region of a Ramachandran plot. The model predicts that the TM segments form a helical bundle, which under nonenergized conditions lines a central water-filled chamber with access to the extracellular space. Corresponding TM segments of different monomers show rotational symmetry with an axis perpendicular to the membrane plane. Figure 6 shows a side view of the model. This model reveals that TMs 3, 5, and 6 have broad access to the central cavity, whereas the access of TM segments 2 and 4 is restricted. TM1 forms part of the lining of the central pore at the extracytoplasmic face.

Linking the Substrate Affinity Labeling Pattern to the 3D Structure of LmrA. A close-up view of the TMD is shown in the right part of Fig. 6. In this representation, the TMD is rotated counter clockwise with respect to the side view of the complete model at left and tilted toward the observer. Helices are numbered 1 to 6 for the monomer, which lies to the front and left, and 1′ to 6′ for the other monomer. The close spatial proximity of TMs 5 and 6 of the first monomer can be appreciated at this viewing angle. TM3 of the same monomer is located at the left and quite remote from helices 5 and 6. However, TM 3′ of the other monomer is in close contact with TMs 5 and 6. Thus, labeling data suggest that two rotationally symmetric substrate binding domains are formed by TM segment 3 of one monomer and TMs 5 and 6 of the opposing monomer. TM segments composing the substrate binding domain, which lies closer to the observer, are identified by red numbers in Fig. 6. The spatial proximity of helix 3′ of the right monomer and 5 and 6 of the left monomer is easily seen at this viewing angle. Because helices 3, 5, and 6 are the only TM segments labeled in the nonenergized, the energized, and the posthydrolytic state, the spatial vicinity of these helices seems to be preserved during the transport cycle.

Discussion

The bacterial ABC-multidrug transporter LmrA is functional as a homodimer. It has been demonstrated to have two allosterically interacting substrate-binding sites, one with high affinity and one with low affinity (van Veen et al., 2000). In the transport process, substrates are picked up from the inner leaflet of the membrane and translocated to the external medium (Bolhuis et al., 1996). An alternating two-site model for LmrA (van Veen et al., 2000) postulates that during catalysis, hydrolysis of ATP by the NBD of one half of LmrA is coupled to the movement of an inside-facing, high-affinity drug-binding site to the outside of the membrane with a concomitant change to low affinity and release of the drug into the extracellular medium. In the ADP/vanadate-trapped transition state, only the low-affinity drug-binding site is accessible, whereas the high affinity site is occluded. LmrA has previously been shown by ATR-FTIR studies to pass through different conformational states during its catalytic cycle (Vigano et al., 2000), which provides a possible explanation for these affinity changes. For P-glycoprotein, evidence has been presented that for iodoarylazidoprazosine, an affinity decrease is brought about by ATP-hydrolysis, requiring the formation of a catalytic transition state (Ramachandra et al., 1998). In contrast, Martin et al. (2001) presented evidence that ATP-binding suffices to bring about a decrease in affinity toward the P-gp substrate vinblastine. Figure 7 summarizes our data obtained by propafenone-type substrate-labeling of LmrA in diagrammatic form. On basis of quantitative and qualitative labeling patterns, three different conformational states of LmrA can be discriminated. These are designated states 1, 2, and 3. State 1 conforms to

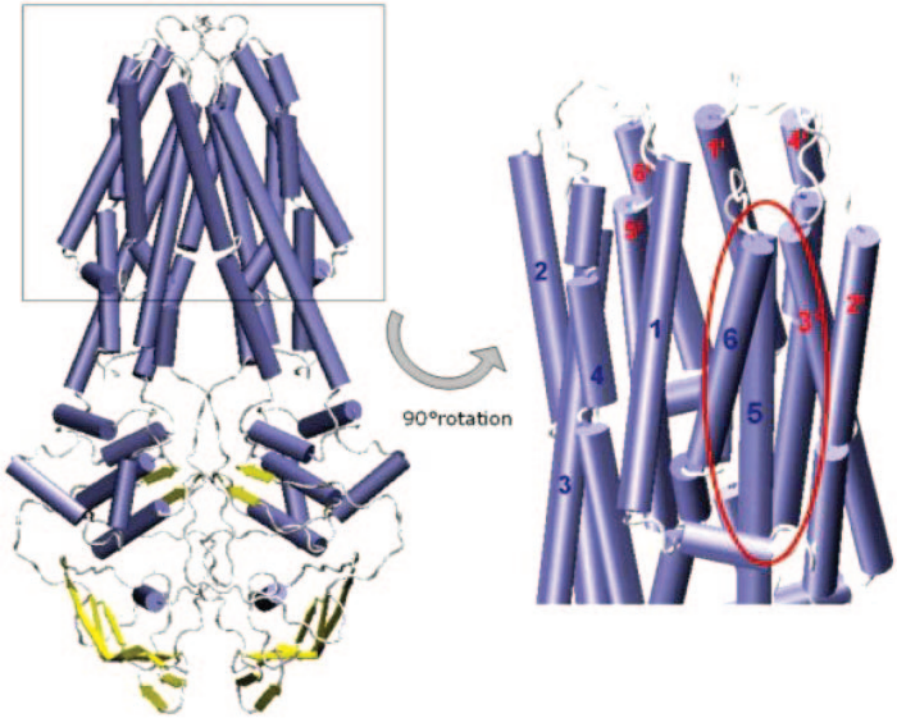

Fig. 6. 3D atomic model of LmrA generated by the software package Insight II, using *V. cholerae* MsbA as the template structure. A side view of the model is shown at the left. Helices are depicted in blue, and β-strands are in yellow. The boxed part indicates the TMD, which is shown in a close-up view at the right (rotated by approximately 90° and tilted toward the observer). The short helix, which is located in an almost horizontal position at front (perpendicular to helix1) gives the approximate location, where the inner leaflet of the membrane borders on the cytoplasm. TM segments of different monomers are numbered 1 to 6 (blue) and 1′ to 6′ (red). The substrate binding domain closer to the observer is circled in red and is composed of TM segments 5 and 6 of one monomer and TM3′ of the other monomer.

the nonenergized state, state 2 to the nucleotide-bound state, and state 3 to the posthydrolytic transition state. Labeling of the intact protein with [^{3}H]GPV51 does not differ significantly between the nonenergized and the nucleotide bound state but decreases to approximately 25% in the posthydrolytic transition state, indicating that in agreement with data from Ramachandra et al. (1998), the decrease in substrate affinity is brought about by ATP hydrolysis and not by ATP binding (Fig. 3). Nevertheless, these three different states of the catalytic cycle correspond to different conformational states of the protein and these are reflected by quantitative changes in labeling of TM segments 5 and 6. These changes are shown as labeling traces. Note that in all cases, changes in TM5 and -6 are inverse. This indicates an alternate involvement of helices 5 and 6 in substrate interaction.

The three dimensional atomic detail model of LmrA was generated on the basis of the template structure of the dimeric lipid A transporter MsbA from *V. cholerae* (see *Materials and Methods*). LmrA and MsbA have been identified as close relatives with overlapping substrate and modulator profiles (Reuter et al., 2003).

In this study, the substrate binding domain of LmrA has been characterized in greater detail by use of propafenone-derived substrate photo-ligands. It seems important to note at this point that photoaffinity labeling is driven by photochemical reactivity. Although the approach is ideally suited to identify regions of ligand binding, photochemically reacting amino acid residues are not necessarily involved in the physiology of ligand-protein interaction.

Data reveal that propafenones bind to discrete regions of LmrA in TM segments 3, 5, and 6. Recently, we showed that TM segments 5 and 6 are involved in binding of an LmrA substrate in the nonenergized state (Alqwai et al., 2003). A 6.8-kDa fragment of LmrA, obtained by a *Staphylococcus aureus* V8 protease digest, was shown to bind the substrate iodo-aryl azido Rhodamine123. The 6.8-kDa peptide fragment spans the entire TM5 and -6 (Ala252-Glu314), suggesting that Rh123 and propafenones share at least part of a common binding domain.

The atomic detail three-dimensional model of LmrA seems to represent a valid structure, because all amphipathic helices face the membrane environment with their apolar residues, whereas polar side chains are oriented toward the aqueous environment of a central pore. Helices 3, 5, and 6, which contribute to substrate binding, have broad access to the central cavity. For TM6, these results are consistent with those of cysteine mutagenesis combined with cysteine accessibility studies, which revealed that one half of TM6 is exposed to a cytoplasmic exposed water-filled cavity along the whole length of the α-helix (Poelarends and Konings, 2002).

In contrast, helices 1, 2, and 4, which do not participate in ligand binding, are predicted to have limited access to the central pore. The LmrA-model indicates close spatial proximity between TM3 of one monomer with TMs 5 and 6 of the other monomer (see Fig. 6), thus allowing the formation of two rotationally symmetric drug binding domains at the monomer/monomer interfaces.

Labeling at different steps of the transport cycle revealed that in the nonenergized state, the AMP-PNP bound state, and in the posthydrolytic transition state, labeling remained confined to TM segments 3, 5, and 6. Although the LmrA model represents a snapshot of the protein in the nonenergized state, data suggest that substrate-binding helices stay in close contact to each other during the catalytic cycle. Although qualitative changes were thus not observed, the labeling intensity of TM segments 5 and 6 changed in the

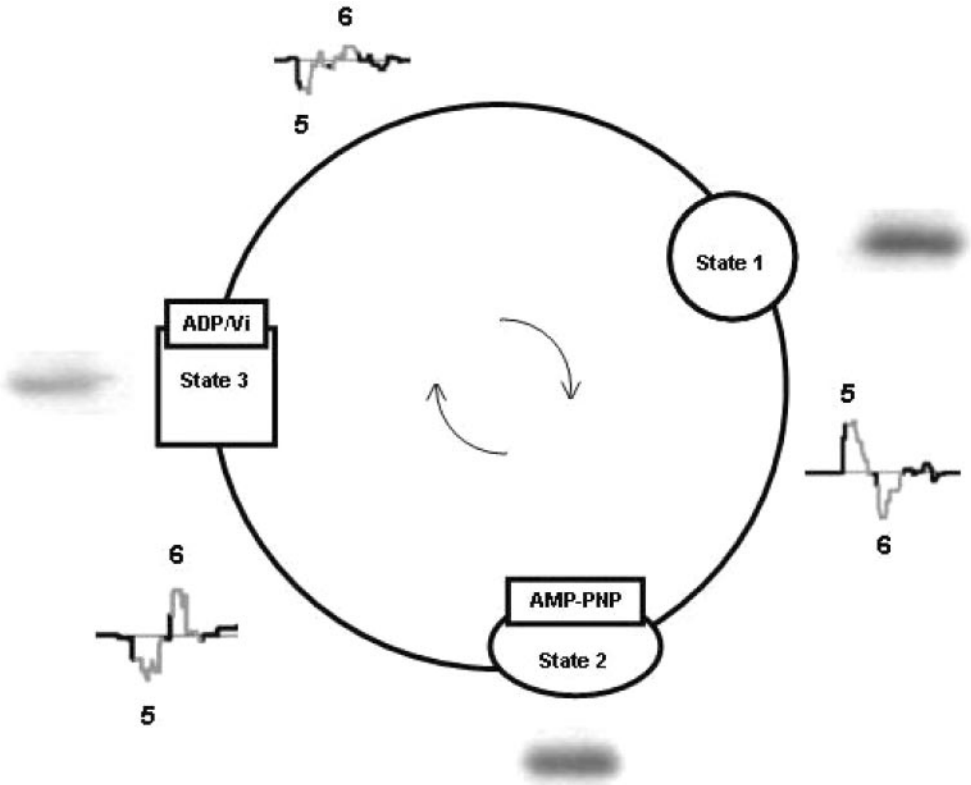

Fig. 7. Diagrammatic representation of photoaffinity labeling data. On basis of quantitative and qualitative labeling patterns, three different conformational states of LmrA are apparent, that are designated states 1, 2, and 3. State 1 conforms to the nonenergized state, state 2 to the nucleotide-bound state, and state 3 to the posthydrolytic transition state. Labeling of the intact protein with [^{3}H]GPV51 is shown as the LmrA band intensity in fluorographs next to the conformational state. The substrate affinity decrease is clearly the result of ATP hydrolysis and not of ATP binding. Quantitative changes in labeling of TM segments 5 and 6 between different states are shown as labeling traces (see Fig. 4). Note that in all cases, changes in TM5 and -6 are inverse, indicating an alternate involvement of helices 5 and 6 during transport.

course of the transport cycle (Figs. 4 and 5). Data in Fig. 4 show that highest changes in labeling were centered on amino acid positions Leu268 in TM5 and Tyr297 in TM6. The LmrA model predicts these residues to be located at the monomer/monomer interface at positions that are close to the border between inner and outer leaflet of the membrane. Inverse changes in the ligand accessibility of TM5 and TM6 and the proximity of residues Leu268 and Tyr297 as well as a similar orientation suggest that during the transport cycle, helices 5 and 6 might reposition relative to TM3. Binding of substrates at interfaces might represent a paradigm for multidrug transporters, because cocrystallization of acrB, a proton motive force-dependent multidrug transporter from *E. coli*, with its substrates rhodamine 6G, dequalinium, ethidium, and ciprofloxacin, revealed that substrates can be bound at the trimer interfaces at the outer surface of the membrane (Yu et al., 2003). It is not known whether other binding regions in monomeric acrB are involved in the translocation of substrate from the inside or the inner leaflet to the outer surface.

TM6 is physically tethered to the NBD via a region referred to as the intracellular domain 3 (ICD3) in the MsbA template structure. On the other hand, TM5 is connected to the intracellular domain 2 (ICD2), which is partially unresolved in the crystal structure, indicating the highly flexible nature of this protein region. Both ICD2 and ICD3 represent candidates for the transmission of conformational changes from the NBD to the transmembrane domain, thus enabling substrate translocation. The resolved α-helical portion of ICD2 reaches down toward the α-helical domain of the NBD, indicating that in the native protein, a flexible contact between TMD and NBD is formed in this region. Such a topology is consistent with the finding that the α-helical domain is a region of labeling with the substrate photoaffinity ligands. Likewise, Borchers et al. (2002) identified a peptide fragment spanning Glu468 to Arg527 of P-glycoprotein as being involved in dexniguldipine binding. The identified peptide fragment comprises the α-helical domain of the amino-terminal NBD with the exclusion of the signature motif, which in P-gp is located at amino acid positions Leu531 to Gln535.

In conclusion, the present study was able to define the binding domain of propafenone-type LmrA substrates on basis of interacting peptide fragments and to demonstrate for the first time quantitative changes in the affinity-labeling pattern of an ABC transporter during the course of the transport cycle. This provides an important first step to link static structural information as obtained by protein homology modeling to the dynamics of the transport process. Because multidrug transporters represent important molecular drug targets, these studies will aid in the development of therapeutics used to treat infectious disease and cancer.

Acknowledgments

The contribution of Margreet Moes in performing the inhibition studies of Hoechst transport by propafenones and the assistance of Piotr Mazurkiewizc are greatly appreciated.

References

Al-Shawi MK, Polar MK, Omote H, and Figler RA (2003) Transition state analysis of the coupling of drug transport to ATP-hydrolysis by P-glycoprotein. *J Biol Chem* **278:**52629–52640.

Alqwai O, Poelarends G, Konings WN, and Georges E (2003) Photoaffinity labeling under non-energized conditions of a specific drug-binding site of the ABC multidrug transporter LmrA from *Lactococcus lactis*. *Biochem Biophys Res Commun* **311:**696–701.

Austin EA, Graves JF, Hite LA, Parker CT, and Schnaitman CA (1990) Genetic analysis of lipopolysaccharide core biosynthesis by *Escherichia coli* K-12: insertion mutagenesis of the rfa locus. *J Bacteriol* **172:**5312–5325.

Bolhuis H, van Veen HW, Brands JR, Putman M, Poolman B, Driessen AJ, and Konings WN (1996) Energetics and mechanism of drug transport mediated by the lactococcal multidrug transporter LmrP. *J Biol Chem* **271:**24123–24128.

Borchers C, Boer R, Klemm K, Figala V, Denzinger T, Ulrich WR, Haas S, Ise W, Gekeler V, and Przybylski M (2002) Characterization of the dexniguldipine binding site in the multidrug resistance-related transport protein P-glycoprotein by photoaffinity labeling and mass spectrometry. *Mol Pharmacol* **61:**1366–1376.

Campbell JD, Biggin PC, Baaden M, and Sansom MS (2003) Extending the structure of an ABC transporter to atomic resolution: modeling and simulation studies of MsbA. *Biochemistry* **42:**3666–3673.

Chang G and Roth CB (2001) Structure of MsbA from *E. coli*: a homolog of the multidrug resistance ATP binding cassette (ABC) transporters. *Science (Wash DC)* **293:**1793–1800.

Chang G (2003) Structure of MsbA from *Vibrio cholera*: a multidrug resistance ABC transporter homolog in a closed conformation. *J Mol Biol* **330:**419–430.

Chiba P, Burghofer S, Richter E, Tell B, Moser A, and Ecker G (1995) Synthesis, pharmacologic activity and structure-activity relationships of a series of propafenone-related modulators of multidrug resistance. *J Med Chem* **38:**2789–2793.

Chiba P, Ecker G, Schmid D, Drach J, Tell B, Goldenberg S, and Gekeler V (1996) Structural requirements for activity of propafenone-type modulators in P-glycoprotein-mediated multidrug resistance. *Mol Pharmacol* **96:**1122–1130.

Clauser KR, Baker P, and Burlingame AL (1999) Role of accurate mass measurement (±10 ppm) in protein identification strategies employing MS or MS/MS and database searching. *Anal Chem* **71:**2871–2882.

de Ruyter PG, Kuipers OP, and de Vos WM (1996) Controlled gene expression systems for *Lactococcus lactis* with the food-grade inducer nisin. *Appl Environ Microbiol* **62:**3662–3667.

Durauer A, Csaszar E, Mechtler K, Jungbauer A, and Schmid E (2000) Characterisation of the rubber elongation factor from ammoniated latex by electrophoresis and mass spectrometry. *J Chromatogr A* **890:**145–158.

Ecker G, Csaszar E, Kopp S, Plagens B, Holzer W, Ernst W and Chiba P (2002) Identification of ligand-binding regions of P-glycoprotein by activated-pharmacophore photoaffinity labeling and matrix-assisted laser desorption/ionization-time-of-flight mass spectrometry. *Mol Pharmacol* **61:**637–648.

Gottesman MM and Pastan I (1993) Biochemistry of multidrug resistance mediated by the multidrug transporter. *Annu Rev Biochem* **62:**385–427.

Grimard V, Vigano C, Margolles A, Wattiez R, van Veen HW, Konings WN, Ruysschaert JM and Goormaghtigh E (2001) Structure and dynamics of the membrane-embedded domain of LmrA investigated by coupling polarized ATR-FTIR spectroscopy and $^{1}H/^{2}H$ exchange. *Biochemistry* **40:**11876–11886.

Locher KP, Lee AT, and Rees DC (2002) The *E. coli* BtuCD structure: a framework for ABC transporter architecture and mechanism. *Science (Wash DC)* **296:**1091–1098.

Loo TW and Clarke DM (2001) Cross-linking of human multidrug resistance P-glycoprotein by the substrate, tris-(2-maleimidoethyl)amine, is altered by ATP hydrolysis. Evidence for rotation of a transmembrane helix. *J Biol Chem* **276:**31800–31805.

Loo TW, Bartlett MC, and Clarke DM (2003) Substrate-induced conformational changes in the transmembrane segments of human P-glycoprotein: direct evidence for the substrate-induced fit mechanism for drug binding. *J Biol Chem* **278:**13603–13606.

Loo TW and Clarke TM (2002) Vanadate trapping at the ATP-binding sites of human multidrug resistance P-glycoprotein exposes different residues to the drug binding site. *Proc Natl Acad Sci USA* **99:**3511–3516.

Margolles A, Putman M, van Veen HW, and Konings WN (1999) The purified and functionally reconstituted multidrug transporter LmrA of *Lactococcus lactis* mediates the transbilayer movement of specific fluorescent phospholipids. *Biochemistry* **38:**16298–16306.

Martin C, Higgins CF, and Callaghan R (2001) The vinblastine binding site adopts high- and low-affinity conformations during a transport cycle of P-glycoprotein. *Biochemistry* **40:**15733–15742.

Pleban K, Macchiarulo G, Constantino G, Pelliciari R, Chiba P, and Ecker GF (2004) Homology model of the multidrug transporter LmrA from *Lactococcus lactis*. *Bioorg Med Chem Letters*, in press

Poelarends GJ, Mazurkiewicz P, Putman M, Cool RH, Veen HW, and Konings WN (2000) An ABC-type multidrug transporter of *Lactococcus lactis* possesses an exceptionally broad substrate specificity. *Drug Resist Updat* **3:**330–334.

Poelarends GJ and Konings WN (2002) The transmembrane domains of the ABC multidrug transporter LmrA form a cytoplasmic exposed, aqueous chamber within the membrane. *J Biol Chem* **277:**42891–84289.

Putman M, Van Veen HW, Degener JE, and Konings WN (2000) Antibiotic resistance: era of the multidrug pump. *Mol Microbiol* **36:**772–773.

Ramachandra M, Ambudkar SV, Chen D, Hrycyna CA, Dey S, Gottesman MM, and Pastan I (1998) Human P-glycoprotein exhibits reduced affinity for substrates during a catalytic transition state. *Biochemistry* **37:**5010–5019.

Reuter G, Janvilisri T, Venter H, Shahi S, Balakrishnan L, and van Veen HW (2003) The ATP binding cassette multidrug transporter LmrA and lipid transporter MsbA have overlapping substrate specificities. *J Biol Chem* **278:**35193–35198.

Rihakova L, Deraet M, Auger-Messier M, Perodin J, Boucard AA, Guillemette G, Leduc R, Lavigne P, and Escher E (2002) Methionine proximity assay, a novel method for exploring peptide ligand-receptor interaction. *J Recept Signal Transduct Res* **22:**297–313.

Rosenberg MF, Velarde G, Ford RC, Martin C, Berridge G, Kerr ID, Callaghan R, Schmidlin A, Wooding C, Linton KJ, et al. (2001) Repacking of the transmembrane

domains of P-glycoprotein during the transport ATPase cycle. *EMBO J* **20:**5615–5625.
Rosenberg MF, Kamis AB, Callaghan R, Higgins CF, and Ford RC (2003) Three-dimensional structures of the mammalian multidrug resistance P-glycoprotein demonstrate major conformational changes in the transmembrane domains upon nucleotide binding. *J Biol Chem* **278:**8294–8299.
Sauna ZE and Ambudkar SV (2001) Characterization of the catalytic cycle of ATP-hydrolysis by human P-glycoprotein. The two ATP hydrolysis events in a single catalytic cycle are kinetically similar but affect different functional outcomes. *J Biol Chem* **276:**11653–11661.
Schmitt L and Tampe R (2002) Structure and mechanism of ABC transporters. *Curr Opin Struct Biol* **12:**754–760.
Shevchenko A, Wilm M, Vorm O, and Mann M (1996) Mass spectrometric sequencing of proteins silver-stained polyacrylamide gels. *Anal Chem* **68:**850–858.
van Veen HW, Venema K, Bolhuis H, Oussenko I, Kok J, Poolman B, Driessen AJ, and Konings WN (1996) Multidrug resistance mediated by a bacterial homolog of the human multidrug transporter MDR1. *Proc Natl Acad Sci USA* **93:**10668–10672.
van Veen HW, Callaghan R, Soceneantu L, Sardini A, Konings WN, and Higgins CF (1998) A bacterial antibiotic-resistance gene that complements the human multidrug-resistance P-glycoprotein gene. *Nature (Lond)* **391:**291–295.
van Veen HW, Margolles A, Muller M, Higgins CF, and Konings WN (2000) The homodimeric ATP-binding cassette transporter LmrA mediates multidrug transport by an alternating two-site (two-cylinder engine) mechanism. *EMBO J* **19:**2503–2514.
Vigano C, Margolles A, van Veen HW, Konings WN, and Ruysschaert JM (2000) Secondary and tertiary structure changes of reconstituted LmrA induced by nucleotide binding or hydrolysis. A Fourier transform attenuated total reflection infrared spectroscopy and tryptophan fluorescence quenching analysis. *J Biol Chem* **275:**10962–10967.
Yu EW, McDermott G, Zgurskaya HI, Nikaido H, and Koshland DE Jr (2003) Structural basis of multiple drug-binding capacity of the AcrB multidrug efflux pump. *Science (Wash DC)* **300:**976–980.

Address correspondence to: Peter Chiba, Institute of Medical Chemistry, Medical University of Vienna, Waehringerstrasse 10, A-1090 Vienna, Austria. E-mail: peter.chiba@univie.ac.at